Explaining inter-annual variability of gross primary productivity from plant phenology and physiology

Sha Zhou, Yao Zhang, Kelly Caylor, Yiqi Luo, Xiangming Xiao, Philippe Ciais, Yuefei Huang, Guangqian Wang

Explaining inter-annual variability of gross primary productivity from plant phenology and physiology

Sha Zhou[1,2], Yao Zhang[3], Kelly K. Caylor[2], Yiqi Luo[4,5], Xiangming Xiao[3,6], Philippe Ciais[7], Yuefei Huang[1,8], Guangqian Wang[1]

[1]State Key Laboratory of Hydroscience and Engineering, Department of Hydraulic Engineering, Tsinghua University, Beijing 100084, China

[2]Department of Civil and Environmental Engineering, Princeton University, Princeton, NJ 08544, USA

[3]Department of Microbiology and Plant Biology, Center for Spatial Analysis, University of Oklahoma, Norman, OK 73019, USA

[4]Department of Microbiology and Plant Biology, University of Oklahoma, Norman, Oklahoma 73019, USA

[5]Center for Earth System Science, Tsinghua University, Beijing 100084, China

[6]Institue of Biodiversity Science, Fudan University, Shanghai 200433, China

[7]Laboratoire des Sciences du Climat et de l'Environnement, CEA CNRS UVSQ, Gif-sur-Yvette 91190, France

[8]College of Ecological and Environmental Engineering, Qinghai University, Xining 810086 Qinghai, China

Correspondence to: Sha Zhou (zhous13@mails.tsinghua.edu.cn) and Yuefei Huang (yuefeihuang@tsinghua.edu.cn)

Abstract

Climate variability influences both plant phenology and physiology, resulting in inter-annual variation in terrestrial gross primary productivity (GPP). However, it is still difficult to explain the inter-annual variability of GPP. In this study, we propose a Statistical Model of Integrated Phenology and Physiology (SMIPP) to explain the contributions of maximum daily GPP (GPP_{max}), and start and end of the growing season (GS_{start} and GS_{end}) to the inter-annual variability of GPP observed at 27 sites across North America and Europe. Strong relationships are found between the anomalies of GS_{start} and spring GPP (r=0.82±0.10), GPP_{max} and summer GPP (r=0.90±0.14), and GS_{end} and autumn GPP (r=0.75±0.18) within each site. Partial correlation analysis further supports strong correlations of annual GPP with GS_{start} (partial r value being 0.72±0.20), GPP_{max} (0.87±0.15), and GS_{end} (0.59±0.26), respectively. In addition, the three indicators are found independent from each other to influence annual GPP at most of the 27 sites. Overall, the site-calibrated SMIPP explains 90±11% of the annual GPP variability among the 27 sites. In general, GPP_{max} contributes to GPP variation more than the two phenological indicators. These results indicate that the inter-annual variability of GPP can be effectively estimated using the three indicators. Investigating plant physiology, and spring and autumn phenology to environmental changes can improve the prediction of the annual GPP trajectory under future climate change.

Keywards: daily maximum GPP, start of growing season, end of growing season, climate change, drought

1. Introduction

Global carbon cycle exhibits strong inter-annual variability, most of which has been inferred to be caused by changes in carbon sequestration in terrestrial ecosystems (Ballantyne *et al.*, 2012). Indeed, the inter-annual variability is one of the least understood carbon cycle processes (Luo *et al.*, 2015). Past researches have been focused on the timings of spring emergence and autumn senescence under global warming, which were found to shift in the Northern Hemisphere, and the length of growing season has changed (Cleland *et al.*, 2007; Ibáñez *et al.*, 2010). Growing season length has substantial effects on annual carbon uptake; both gross primary productivity (GPP) and net ecosystem productivity (NEP) are enhanced by longer growing seasons caused by warming climate (Churkina *et al.*, 2005; Dragoni *et al.*, 2011; Keenan *et al.*, 2014; Piao *et al.*, 2007; Richardson *et al.*, 2010). In addition, warming-induced drought stress limits plant photosynthesis in summer and leads to great decline in peak summer productivity and even annual GPP (Angert *et al.*, 2005; Buermann *et al.*, 2013; Ciais *et al.*, 2005; Schwalm *et al.*, 2012). Since both phenology dates and photosynthetic physiology greatly affect annual GPP, it is necessary to explain annual GPP variability from both plant phenology and physiology yet to partition their respective contributions.

Recently, Xia *et al.* (2015) proposed that annual GPP is jointly controlled by plant phenology and physiology and can be diagnosed by the product of the length of CO_2 uptake period (CUP) and the maximum capacity of CO_2 uptake (GPP_{max}). The product of CUP and GPP_{max}, i.e., CUP $\times$ GPP_{max}, can explain more than 90% of the temporal GPP variability in most areas of North America during 2000-2010 and more than 95% of the spatial GPP variation among 213 flux tower sites. Although CUP is a good phenological indicator, it does not allow us to separately evaluate the influence of spring and autumn phenology on annual GPP variability. While CUP

64 does not change, spring emergence and autumn senescence may shift and affect annual GPP in
65 different ways (Richardson *et al.*, 2010). In addition, the respective contributions of spring
66 emergence and autumn senescence to growing season change and hence annual GPP variability
67 have not been separated, and their contributions seem to vary across different ecosystems
68 (Garonna *et al.*, 2014; Jeong *et al.*, 2011; Menzel & Fabian, 1999; Zhu *et al.*, 2012). Thus, the
69 effects of both spring emergence and autumn senescence on annual GPP should be considered
70 separately to investigate the contributions of spring and autumn phenological changes to the
71 inter-annual variability of GPP.

72 In northern temperate ecosystems, the growing season starts in spring and ends in autumn when
73 the photosynthetic carbon assimilation is limited by temperature and solar radiation. Daily
74 photosynthetic rate reaches its peak (GPP_{max}) in summer under favorable environmental
75 conditions, and GPP is small or even negligible in winter (Allard *et al.*, 2008; Hirata *et al.*, 2007;
76 Saigusa *et al.*, 2008; Uehlinger, 2006). The starting and ending dates of the growing season,
77 expressed by GS_{start} and GS_{end}, are closely correlated with spring and autumn GPP, respectively
78 (Keenan *et al.*, 2014). Similarly, GPP_{max} is positively correlated with summer GPP (Stoy *et al.*,
79 2014). Thus, the three indicators, GS_{start}, GPP_{max}, and GS_{end}, can influence seasonal GPP and
80 hence annual GPP. Combining the effects of these three indicators, it may have the potential to
81 explain annual GPP variability and separate the respective contributions of both spring and
82 autumn phenology and plant physiology to it.

83 Because the phenological and physiological events occur in different seasons and affect carbon
84 assimilation in different ways, these three indicators may have independent effects on annual
85 GPP. The spring emergence and autumn senescence dates vary temporally and spatially, and
86 respond differently to climate change (Vitasse *et al.*, 2009). Although there is a strong

correlation between warmer temperature and earlier spring emergence, the association between temperature and autumn senescence is weaker (Menzel *et al.*, 2006). In addition to temperature, spring emergence is also affected by other factors, such as winter chilling conditions and freeze-thaw processes (Chen *et al.*, 2011; Fu *et al.*, 2015; Pope *et al.*, 2013; Yi & Zhou, 2011; Yu *et al.*, 2010). Autumn senescence has been reported to be influenced by multiple factors, including temperature, precipitation, photoperiod, soil moisture, wind, frost events, etc. (Fracheboud *et al.*, 2009; Panchen *et al.*, 2015; Yang *et al.*, 2015). In view of the different responses to climate factors, both spring emergence and autumn senescence should be included and the combination of the three indicators could provide more exhaustive explanation of annual GPP variability.

This paper proposes an integrated statistical model to explain the inter-annual variability of GPP in the Northern Hemisphere from the perspectives of both phenology and physiology and evaluates the contributions of phenological and physiological changes to annual GPP variability using data from 27 flux tower sites (283 site-years) across North America and Europe. The specific objectives are to (1) investigate the effects of variations in GS_{start}, GPP_{max} and GS_{end} on respective seasonal GPP and hence annual GPP; (2) develop a Statistical Model of Integrated Phenology and Physiology (SMIPP) involving the three indicators to explain the inter-annual variability of GPP for each site; (3) partition the contributions of phenological and physiological changes to annual GPP variability for the 283 site-years.

2. Materials and Methods

2.1 Flux tower data

GPP estimates (g $C \cdot m^{-2} \cdot day^{-1}$) were obtained from 14 AmeriFlux sites and 13 EuroFlux sites (Table 1). A total of 283 site-years were used and the record length for each site ranged from 6 to

21 years. Generally, the 27 flux sites were classified into three plant functional types, including 8 deciduous broadleaf forests (DBF), 9 evergreen needle-leaf forests (ENF), and 10 non-forests sites (NF) (e.g., cropland, grassland, closed shrubland and wetland). The estimates of GPP were available from AmeriFlux (Level 2 products, http://public.ornl.gov/ameriflux) and EuroFlux (Level 4 products, http://gaia.agraria.unitus.it/). The half-hourly eddy covariance measurements (i.e., net ecosystem exchange) used in this study have been standardized, gap-filled using the Marginal Distribution Sampling (MDS) method, and partitioned into GPP and ecosystem respiration (Papale & Valentini, 2003; Reichstein *et al.*, 2005).

The 27 sites were chosen according to the following four criteria. (1) The site-years with more than 80% of the GPP data were actual measurements or gap-filled with high confidence, i.e., data marked as 'the original' or 'most reliable' according to the quality flag, were selected. Only the site-years with effective measurements covering the entire growing season (March-October) were used. (2) The sites with at least 6 site-years of data were selected in order to avoid overfitting of multiple linear regression. According to Austin and Steyerberg (2015), a minimum of two observations per variable is required to permit accurate estimation of regression coefficients (relative bias<10%). As three variables (GS_{start}, GPP_{max} and GS_{end}) were used to build up the regression, 6 years of observations for each site is the minimum requirement. (3) Sites located in the moist tropical climate with low seasonality of daily GPP were not used because the phenology dates cannot be identified according to the given threshold. (4) Sites located in some Mediterranean climate were not used because the maximum daily GPP occurs during the winter-spring seasons.

Table 1 Twenty-seven eddy covariance sites in North America and Europe used in this study. Site descriptions include Site Identifier (ID), Latitude (Lat, °), Longitude (Lon, °), Plant

132 Functional Type (PFT), Period of Record, and a reference for each sites. PFTs are taken from the
133 International Geosphere-Biosphere Program (IGBP) land cover classification scheme (DBF =
134 Deciduous Broadleaf Forest, ENF = Evergreen Needle-Leaf Forest, CRO = Cropland, GRA =
135 Grassland, CSH = Closed Shrub Land, WET = Wetland).

Site ID	Lat	Lon	PFT	Period of Record	Reference
DE-Hai	51.0792	10.4530	DBF	2000-2007	(Kutsch *et al.*, 2008)
IT-Col	41.8494	13.5881	DBF	1998/2000-2002/2005/ 2007-2012	(Valentini *et al.*, 1996)
IT-Ro2	42.3903	11.9209	DBF	2002-2008/2010-2012	(Gioli *et al.*, 2004)
US-Ha1	42.5378	-72.1715	DBF	1992-2012	(Urbanski *et al.*, 2007)
US-MMS	39.3231	-86.4131	DBF	1999-2014	(Dragoni *et al.*, 2007)
US-PFa	45.9459	-90.2723	DBF	1997-2004/2006-2014	(Saito *et al.*, 2009)
US-UMd	45.5625	-84.6975	DBF	2007-2013	(Nave *et al.*, 2011)
US-WCr	45.8060	-90.0798	DBF	1999-2006/2011-2014	(Yi *et al.*, 2004)
BE-Bra	51.3092	4.5206	ENF	1999-2000/2002/2004-2008	(Carrara *et al.*, 2004)
CA-Qcu	49.2671	-74.0365	ENF	2002-2009	(Giasson *et al.*, 2006)
CA-Qfo	49.6925	-74.3420	ENF	2004-2009	(Bergeron *et al.*, 2007)
CH-Dav	46.8153	9.8559	ENF	1998-2009	(Zweifel *et al.*, 2010)
FI-Sod	67.3619	26.6378	ENF	2000-2008	(Thum *et al.*, 2007)
IT-Ren	46.5869	11.4337	ENF	1999/2001-2011	(van Gorsel *et al.*, 2009)
RU-Fyo	56.4615	32.9221	ENF	1999-2010	(Groenendijk *et al.*, 2009)
US-Ho1	45.2041	-68.7402	ENF	1996-2004/2006-2008	(Hollinger *et al.*, 2004)
US-Ho2	45.2091	-68.7470	ENF	1999-2009	(Richardson & Hollinger, 2005)
US-Ne1	41.1650	-96.4766	CRO	2002-2012	(Suyker *et al.*, 2005)
US-Ne2	41.1649	-96.4701	CRO	2001-2012	(Suyker *et al.*, 2005)
US-Ne3	41.1797	-96.4396	CRO	2001-2012	(Suyker *et al.*, 2005)
AT-Neu	47.1167	11.3175	GRA	2002-2009	(Wohlfahrt *et al.*, 2008)
IT-MBo	46.0147	11.0458	GRA	2003-2012	(Gilmanov *et al.*, 2007)
SE-Deg	64.1820	19.5567	GRA	2001-2003/2005-2009	(Lund *et al.*, 2010)

UK-AMo	55.7917	-3.2389	GRA	2003/2005-2010	(Stoy *et al.*, 2013)
US-Kon	39.0824	-96.5603	GRA	2007-2012	(Scurlock *et al.*, 2002)
US-Los	46.0827	-89.9792	CSH	2001-2008	(Liang *et al.*, 2006)
FI-Kaa	69.1407	27.2950	WET	2000-2008	(Aurela *et al.*, 2004)

The half-hourly data of GPP were aggregated to daily totals. The following subsequent steps were taken: (1) seasonal and annual GPP were calculated for each site-year; for seasonal analysis, spring refers to March-May, summer refers to June-August, autumn refers to September-November, and the remaining months are considered as winter; (2) the time series of daily GPP over each site-year were smoothed using singular spectrum analysis (SSA) to identify the three indicators GS_{start}, GPP_{max} and GS_{end}; (3) Pearson correlation was used to develop the relationship between the anomalies of the three indicators and their respective seasonal GPP; Pearson partial correlation was used to develop the relationship between the anomalies of annual GPP and each of three indicators; (4) the interrelationship between each pair of the three indicators was investigated to test whether the three indicators are independent from each other; (5) a multiple regression model was established between the anomalies of annual GPP and the three indicators to explain the inter-annual variability of GPP and separate the contributions of the three indicators for each site.

2.2 A Statistical Model of Integrated Phenology and Physiology

The Statistical Model of Integrated Phenology and Physiology (SMIPP) to explain the inter-annual variability of GPP is an extension of the approach of Xia *et al.* (2015), i.e., $GPP = \alpha \cdot CUP \cdot GPP_{max}$. Firstly, annual GPP is expressed as a function of GS_{start}, GPP_{max}, and GS_{end}

$$GPP = f(GS_{start}, GPP_{max}, GS_{end}) \qquad (1)$$

153 The three indicators GS_{start}, GPP_{max} and GS_{end} are assumed to be independent from each other
154 and that their combination includes the phenological and physiological changes of plants under
155 environmental changes. The total differential form of annual GPP with respect to the three
156 indicators is as follows:

$$dGPP = \frac{\partial GPP}{\partial GS_{start}} dGS_{start} + \frac{\partial GPP}{\partial GPP_{max}} dGPP_{max} + \frac{\partial GPP}{\partial GS_{end}} dGS_{end} \qquad (2)$$

157 Transforming the absolute changes in annual GPP and the three indicators into their relative
158 forms, the relative change in annual GPP can be evaluated as

$$\frac{dGPP}{\overline{GPP}} = \frac{\partial GPP/\overline{GPP}}{\partial GS_{start}/\overline{GS_{start}}} \frac{dGS_{start}}{\overline{GS_{start}}} + \frac{\partial GPP/\overline{GPP}}{\partial GPP_{max}/\overline{GPP_{max}}} \frac{dGPP_{max}}{\overline{GPP_{max}}} + \frac{\partial GPP/\overline{GPP}}{\partial GS_{end}/\overline{GS_{end}}} \frac{dGS_{end}}{\overline{GS_{end}}}$$

159 or

$$\frac{dGPP}{\overline{GPP}} = m_{start} \frac{dGS_{start}}{\overline{GS_{start}}} + m_{gpp} \frac{dGPP_{max}}{\overline{GPP_{max}}} + m_{end} \frac{dGS_{end}}{\overline{GS_{end}}} \qquad (3)$$

160 where $\overline{GS_{start}}$, $\overline{GPP_{max}}$, $\overline{GS_{end}}$ and $\overline{GPP}$ refer to the mean annual values of the three indicators
161 and annual GPP, and are constant for a given site. The parameters m_{start} ($\frac{\partial GPP/\overline{GPP}}{\partial GS_{start}/\overline{GS_{start}}}$), m_{gpp}
162 ($\frac{\partial GPP/\overline{GPP}}{\partial GPP_{max}/\overline{GPP_{max}}}$) and m_{end} ($\frac{\partial GPP/\overline{GPP}}{\partial GS_{end}/\overline{GS_{end}}}$) are the sensitivity coefficients of annual GPP relative
163 to GS_{start}, GPP_{max} and GS_{end}, respectively, representing the conversion factors from the
164 relative changes in the three indicators to the relative change in annual GPP. Equation (3)
165 indicates that the inter-annual variability of GPP can be decomposed into three independent
166 components, induced by the changes in the three indicators. The phenological and physiological
167 sensitivity coefficients of annual GPP in the SMIPP were estimated using the multiple regression
168 method, where $\frac{dGPP}{\overline{GPP}}$ is the dependent variable and $\frac{dGS_{start}}{\overline{GS_{start}}}$, $\frac{dGPP_{max}}{\overline{GPP_{max}}}$, $\frac{dGS_{end}}{\overline{GS_{end}}}$ are the independent
169 variables.

2.3 Determination of phenology and physiology indicators

Values for GS_{start}, GS_{end} and GPP_{max} were determined from time series of GPP for each site-year. Singular spectrum analysis (SSA) was used to derive smoothed curves from daily GPP measurements (Fig. 1). The SSA is a non-parametric method for the analysis of time series. It can decompose a time series into oscillatory components and noises according to the singular value decomposition, and then reconstruct specific components (e.g., seasonal signal) from the original time series (Vautard *et al.*, 1992). The SSA method has been used to identify the phenological transition dates from time series of GPP in previous studies (Keenan *et al.*, 2014). The "Rssa" package in R (https://cran.r-project.org/web/packages/Rssa/index.html) provides a set of fast and reliable tools to perform SSA, and it was used to decompose and reconstruct the time series of GPP and obtain a smoothed curve of daily GPP for each site-year.

GPP_{max} was determined as the peak value of the smoothed curve of daily GPP. GS_{start} and GS_{end} were determined as the first and last days when the smoothed daily GPP crossed a given threshold. In this study, the threshold was set to be 10% of the multi-year average GPP_{max} over all available years for each site, and it varied from 0.5 to 2.5 g $C \cdot m^{-2} \cdot day^{-1}$ among different sites. The choice of this threshold was determined by comparing with other approaches. In comparison with fixed thresholds across all sites (e.g., 2 g $C \cdot m^{-2} \cdot day^{-1}$ in Richardson *et al.* (2010)), relative thresholds for individual sites can better capture variations in phenological events without being affected by different vegetation types and sites, because GPP_{max} varies considerably (5-25 g $C \cdot m^{-2} \cdot day^{-1}$) among different sites. Keenan *et al.* (2014) used 30% of mean annual variance of daily GPP as a threshold for each site, and stated that the inter-annual variability of the derived phenological dates is not affected by the threshold value, which only impacts the mean estimated dates for each site. Compared with a variable threshold, such as 10% of GPP_{max} for each year in

193 Wu *et al.* (2013), a fixed threshold 10% of the multi-year average GPP_{max} for each site used in
194 this study can better reflect the inter-annual variability in phenological transition dates and avoid
195 artificially induced interrelationship among the three indicators.

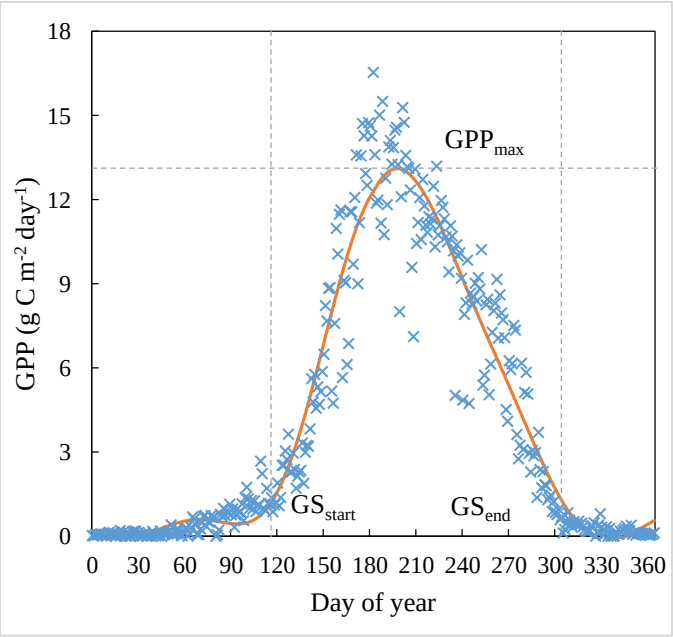

196

197 **Fig. 1.** An example of the reconstructed time series of daily gross primary productivity (GPP)
198 using the singular spectrum analysis method, and determination of the three phenological and
199 physiological indicators, i.e., GS_{start}, GPP_{max} and GS_{end} at the US-Ha1 (DBF) site in 2002.

200 **2.4 Absolute and relative anomaly analyses**

201 An anomaly analysis was performed to represent the inter-annual variability of GPP and other
202 variables. Both the absolute and relative anomalies were used in this study. The absolute
203 anomaly refers to the deviation of a variable from its mean value, while the relative anomaly is
204 the standardized deviation of a variable from its mean value. The two kind of anomalies are
205 calculated as follows:

$$\Delta X_i = X_i - \bar{X} \qquad (4)$$

$$\delta X_i = \frac{X_i - \bar{X}}{\bar{X}} \times 100\% \qquad (5)$$

where X_i represents the variable X in year i, and $\bar{X}$ is the mean annual value of variable X over all the available years for each site. ΔX_i and δX_i represent the absolute and relative anomalies of X_i, respectively. The absolute anomalies of seasonal and annual GPP, and the three indicators GS_{start}, GPP_{max} and GS_{end}, were calculated for correlation analysis. Relative anomalies of the three independent variables and one dependent variable in equation (3) were used to establish the SMIPP for each of the 27 sites.

To make the absolute and relative anomalies of GS_{start} and GS_{end} more comparable, they were calculated in the following ways:

$$\Delta GS_{start} = \overline{GS_{start}} - GS_{start} \qquad (6)$$

$$\Delta GS_{end} = GS_{end} - \overline{GS_{end}} \qquad (7)$$

$$\delta GS_{start} = \frac{\Delta GS_{start}}{\overline{GS_{start}}} \times 100\% \qquad (8)$$

$$\delta GS_{end} = \frac{\Delta GS_{end}}{365 - \overline{GS_{end}}} \times 100\% \qquad (9)$$

The absolute anomalies in equations (6) and (7) would be positive when GS_{start} advances and GS_{end} delays relative to their mean values, which both contribute positively to the annual GPP increase. The relative anomalies of GS_{start} and GS_{end} in equations (8) and (9) were used as the independent variables of the SMIPP in equation (3).

3. Results

3.1 Relationship between the anomalies of GPP and the three indicators

The absolute anomalies of the two phenological indicators, GS_{start} and GS_{end}, and of the physiological indicator, GPP_{max}, were used to explain inter-annual variations in seasonal GPP and hence annual GPP. For example, Fig. 2 shows the relationship between absolute anomalies of the three indicators and corresponding seasonal GPP at the US-Ha1 site. Similarly, the three indicators were used to explain the GPP variability across the three PFTs and the 27 sites.

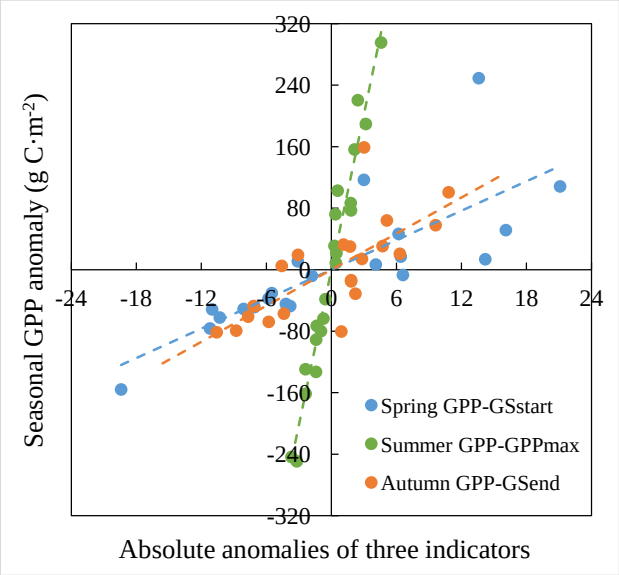

Fig. 2. An example of the linear relationship between the absolute anomalies of GS_{start} (day) and spring GPP, GPP_{max} (g C·m^{-2}·d^{-1}) and summer GPP, GS_{end} (day) and autumn GPP, respectively, at the US-Ha1 site.

The correlation results between the anomalies of the three indicators and their respective seasonal GPP for the 27 sites are shown in Fig. 3. GPP_{max} shows a strong correlation with summer GPP (0.90±0.14), and the correlation coefficient is more than 0.80 for 24 out of the 27 sites, except for two DBF sites (DE-Hai and IT-Ro2) and one NF site (US-Ne1). The two

phenological indicators do not explain spring and autumn GPP variations so well as GPP_{max} explains summer GPP variation. And GS_{start} correlates with spring GPP (r=0.82±0.10) more closely than GS_{end} with autumn GPP (r=0.75±0.18). The linear relationship between GPP_{max} and summer GPP is stronger for ENF (r=0.95±0.03) sites than for DBF (r=0.83±0.20) and NF (r=0.90±0.11) sites. Although GPP_{max} explains summer GPP well for ENF sites, the two phenological indicators explain spring and autumn GPP less well for ENF than for the other two PFTs (Fig. 3a-c). NF sites show the highest correlation coefficients between GS_{start} and spring GPP (0.86±0.08) and between GS_{end} and autumn GPP (0.83±0.11).

The increase in GPP_{max} leads to more carbon assimilation in summer for ENF sites, where 1g $C{\cdot}m^{-2}{\cdot}d^{-1}$ increase in GPP_{max} corresponds to an increase of 79.3±9.2 g $C{\cdot}m^{-2}$ in summer GPP. The sensitivity of summer GPP to GPP_{max} is 84.7±25.0 g $C{\cdot}m^{-2}$ for NF sites and 76.3±25.2 g $C{\cdot}m^{-2}$ for DBF sites (Fig. 3e). On average, a one-day advance in GS_{start} and a one-day delay in GS_{end} increase GPP in spring and autumn by 4.0±2.5 and 4.4±2.6 g $C{\cdot}m^{-2}$, respectively. A one-day change in GS_{start} and GS_{end} causes the largest GPP changes in spring (6.3±1.8 g $C{\cdot}m^{-2}$) and autumn (5.6±1.7 g $C{\cdot}m^{-2}$) for DBF sites. Spring and autumn GPP respond to GS_{start} and GS_{end} in different ways at the NF sites (Fig. 3d and f). A one-day delay in GS_{end} increases GPP by 5.3±3.2 g $C{\cdot}m^{-2}$ in autumn, while a one-day advance in GS_{start} only increases GPP by 2.9±2.5 g $C{\cdot}m^{-2}$ in spring.

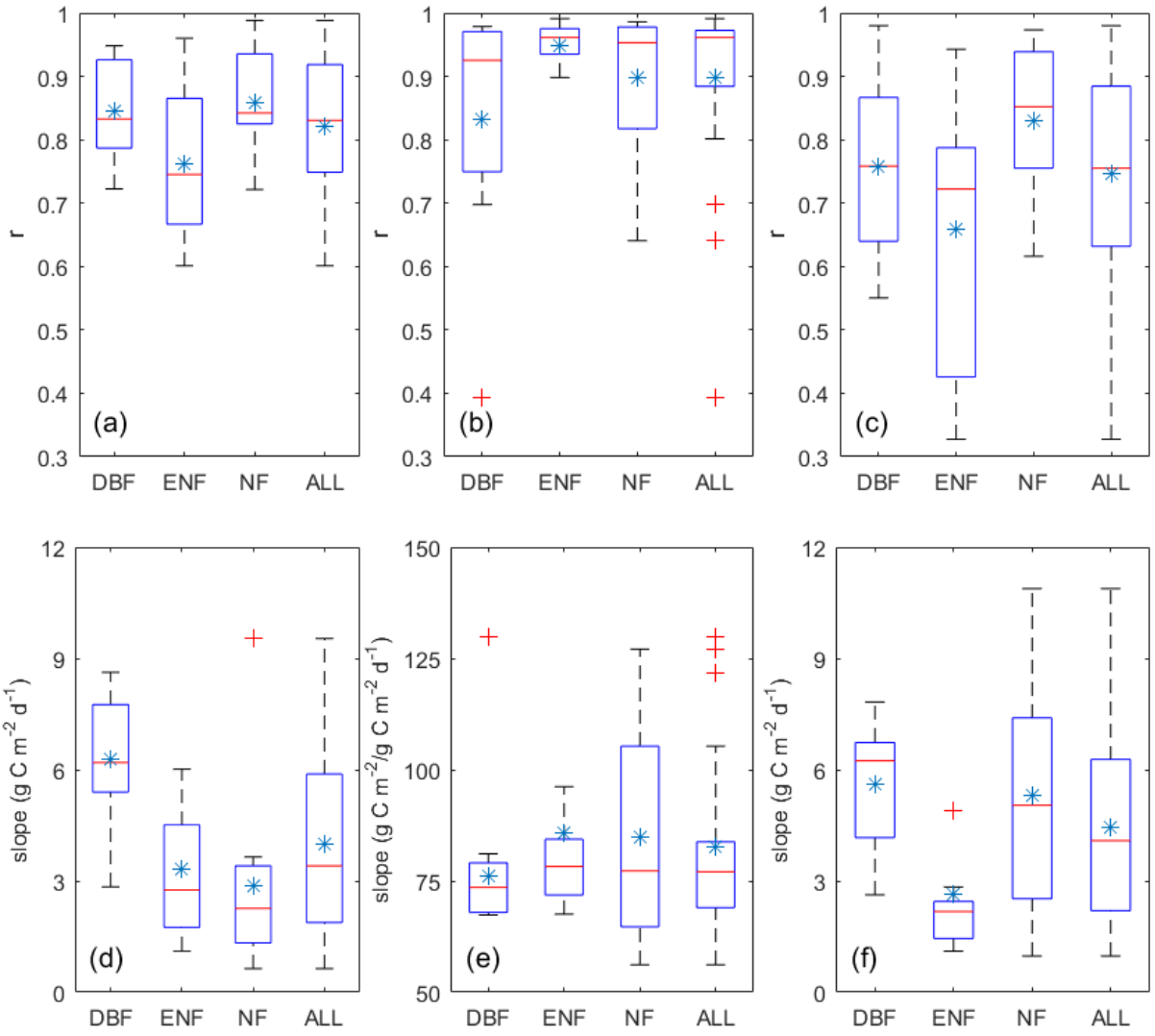

Fig. 3. Distributions of correlation coefficients (r) and regression slopes between the absolute anomalies of (a, d) GS_{start} (day) versus spring GPP (g C·m^{-2}), (b, e) GPP_{max} (g C·m^{-2}·d^{-1}) versus summer GPP, and (c, f) GS_{end} (day) versus autumn GPP for the three PFTs and all of the 27 sites. The mean values of r and regression slopes are shown in asterisks.

The partial correlation analysis between the anomalies of annual GPP and the three indicators shows that annual GPP correlates strongest with GPP_{max} (partial r=0.87±0.15), followed by GS_{start} (partial r=0.72±0.20) and GS_{end} (partial r=0.59±0.26) for the 27 sites (Fig. 4a). The

partial correlation coefficient with respect to GPP_{max} is more than 0.80 for 23 of the 27 sites, and that with respect to GS_{start} and GS_{end} is more than 0.60 for 19 and 14 sites, respectively. The effects of the two phenological indicators on annual GPP vary over different sites, resulting in large standard deviation of the partial regression coefficients. GPP_{max} for the NF sites correlates the best with annual GPP (r=0.95±0.04) excluding the effects of the two phenological indicators. Similarly, both GS_{start} and GS_{end} show stronger partial correlation with annual GPP variation for NF sites than for DBF and ENF sites.

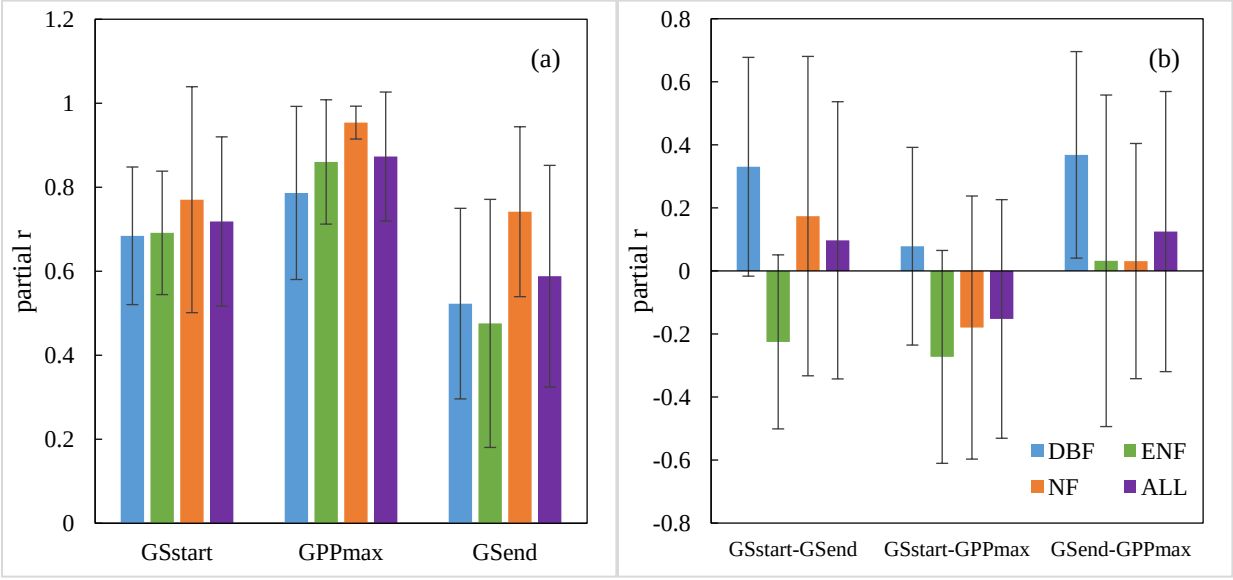

Fig. 4. Partial correlation coefficients (r) (a) between absolute anomalies of annual GPP and the three indicators and (b) between each pair of the three indicators for the three PFTs and all of the 27 sites. The standard deviation of the correlation coefficient is shown in black error bars.

The interrelationships between the three indicators were also investigated for each site. The correlation coefficient is 0.10±0.44 between GS_{start} and GS_{end}, -0.15±0.38 between GS_{start} and GPP_{max}, and 0.12±0.44 between GS_{end} and GPP_{max} (Fig. 4b). Although the interrelationship among the three indicators is strong (with r>0.7 for any pair of correlation) for several sites (3

DBF, 2 ENF and 2 NF sites), the low mean correlation coefficient and high standard deviation indicate that there is no consistent correlation between each pair of the indicators across the 27 sites. As the three indicators individually explain annual GPP variability well, and they are independent from each other to a large extent for most of the 27 sites, the three indicators can be used to establish an integrated statistical model to explain annual GPP variability.

3.2 Statistic model of integrated phenology and physiology for each site

The relative anomalies of the three indicators and annual GPP were calculated and a multiple regression was established to estimate the phenological and physiological sensitivity coefficients in the SMIPP for each of the 27 sites. The coefficients of determination (R^2) of the regression, and the estimated values of the three sensitivity coefficients as well as their significance levels are shown in Table 2. The physiological sensitivity coefficient, m_{gpp}, is significantly different from zero at 0.01 level for 22 sites, and varies from 0.31 to 1.53 and averages at 0.82, indicating that 1 percent change in GPP_{max} would lead to 0.82% change in annual GPP on average (Fig. 5b). Because the two phenological indicators have different effects on annual GPP over different sites, the phenological sensitivity coefficients, m_{start} and m_{end}, show relatively large variability across different sites, ranging from 0.01 to 1.81 and from 0 to 1.39, respectively, and m_{start} is larger than m_{end} for most sites (Fig. 5c and d). Overall, the combination of the three indicators can explain 90±11% of the variation in annual GPP, and the regression equation is significant at 0.01 level for 21 sites, indicating that the SMIPP can explain the inter-annual GPP variability well.

295 **Table 2** Estimated phenological and physiological sensitivity coefficients, i.e., m_{start}, m_{gpp},
296 and m_{end}, and the coefficient of determination (R^2) of the SMIPP for each of the 27 sites. The
297 statistically significance (p-value) of the regression equations and sensitivity coefficients are
298 shown as well.

Site ID	PFT	R^2	p-value	m_{start}	p-value	m_{gpp}	p-value	m_{end}	p-value
DE-Hai	DBF	0.57	0.203	0.99	0.185	0.41	0.390	0.17	0.749
ITCol	DBF	0.90	<0.001	0.75	0.002	0.52	0.056	0.60	0.031
ITRo2	DBF	0.59	0.087	0.81	0.280	0.75	0.040	0.13	0.470
USHa1	DBF	0.93	<0.001	0.61	<0.001	0.64	<0.001	0.48	0.019
USMMS	DBF	0.87	<0.001	0.43	0.011	1.02	<0.001	0.34	<0.001
USPFa	DBF	0.89	<0.001	0.46	0.017	0.63	<0.001	0.17	0.017
USUMd	DBF	0.93	0.008	0.70	0.064	0.87	0.003	0.26	0.118
USWCr	DBF	0.97	<0.001	0.81	<0.001	0.76	<0.001	0.33	0.175
BEBra	ENF	0.87	0.012	0.08	0.211	0.74	0.009	0.03	0.624
CAQcu	ENF	1.00	<0.001	0.52	0.003	0.84	<0.001	0.11	0.347
CAQfo	ENF	0.90	0.054	0.59	0.058	1.33	0.049	0.54	0.079
CHDav	ENF	0.71	0.008	0.21	0.154	0.31	0.127	0.11	0.096
FISod	ENF	0.97	<0.001	0.51	0.028	0.61	0.001	0.00	0.996
ITRen	ENF	0.98	<0.001	0.29	0.011	0.87	<0.001	0.19	0.001
RUFyo	ENF	0.86	<0.001	0.42	0.039	0.86	<0.001	0.18	0.093
USHo1	ENF	0.89	<0.001	0.32	0.022	0.74	0.001	0.13	0.013
USHo2	ENF	0.77	0.006	0.34	0.048	0.56	0.003	0.04	0.600
USNe1	CRO	1.00	<0.001	1.26	<0.001	0.88	<0.001	0.78	<0.001
USNe2	CRO	0.99	<0.001	0.71	0.028	1.03	<0.001	0.56	0.007
USNe3	CRO	0.99	<0.001	1.81	0.001	0.88	<0.001	1.39	0.005
ATNeu	GRA	0.94	0.002	0.15	0.011	1.53	0.003	0.14	0.027

ITMBo	GRA	0.89	0.001	0.60	0.005	1.24	0.002	0.33	0.020
SEDeg	GRA	0.95	0.001	0.17	0.759	0.73	0.005	0.30	0.425
UKAMo	GRA	0.95	0.068	0.38	0.011	0.80	0.002	0.13	0.155
USKon	GRA	0.96	0.012	0.18	0.395	0.87	0.010	0.09	0.439
USLos	CSH	0.98	<0.001	0.75	0.001	0.70	<0.001	0.45	0.002
FIKaa	WET	0.99	<0.001	1.24	<0.001	0.92	<0.001	0.96	0.002

The NF sites consistently exhibit high R^2 (0.96±0.03) in the SMIPP, suggesting that the three indicators can effectively capture the annual GPP change in non-forest ecosystems. In comparison with NF sites, R^2 varies among the ENF (0.88±0.09) and DBF (0.83±0.15) sites (Fig. 5a). The low value and large variance of R^2 at the DBF sites are largely attributed to two sites, i.e., DE-Hai and IT-Ro2, where GPP_{max} does not capture the summer GPP change, especially during drought years, which will be discussed later. The value of m_{gpp} is much larger for NF sites (0.96±0.24) than that for DBF (0.70±0.18) and ENF (0.76±0.26) sites (Fig. 5b), indicating that annual GPP of NF is more sensitive to GPP_{max}. At the NF sites, summer GPP accounts for a larger proportion of annual GPP, thus, 1% change in GPP_{max} would lead to a greater change in annual GPP at the NF sites. The NF sites show high variations in m_{start} and m_{end}, larger than those for the two forest PFTs. In addition, the values of m_{start} and m_{end} are higher for DBF sites, about twice of those for ENF sites (Fig. 5c and d).

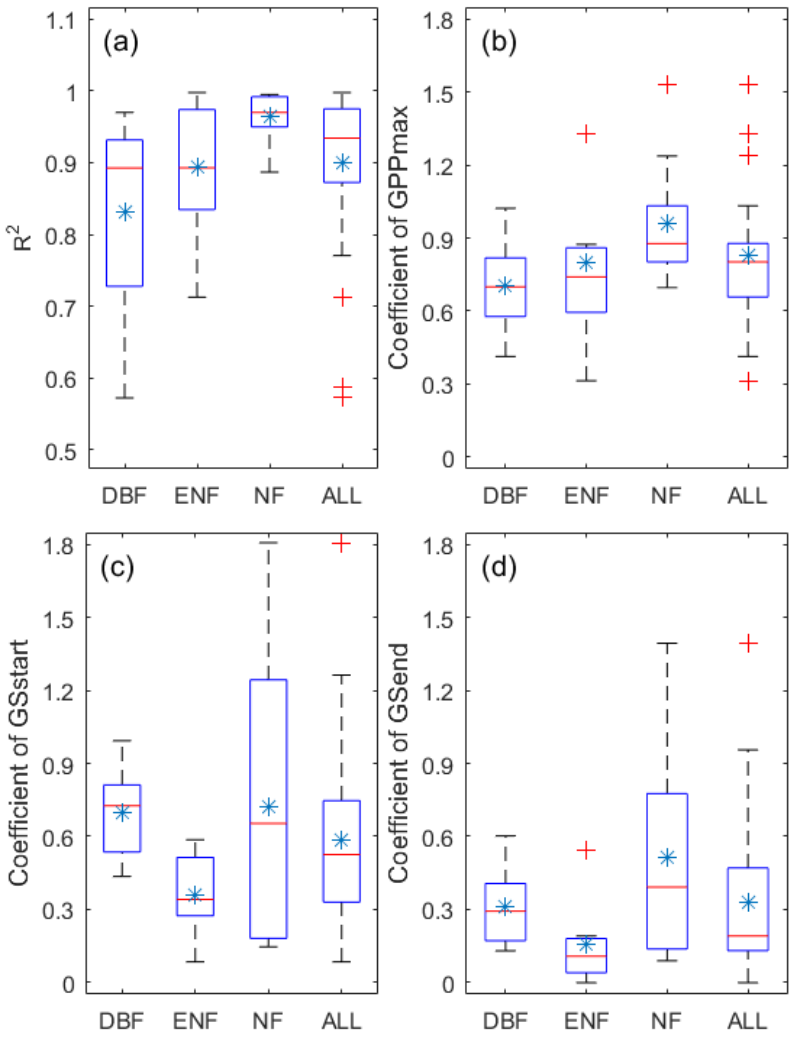

Fig. 5. Distributions of (a) R^2, and the sensitivity coefficients of (b) GPP_{max}, (c) GS_{start}, and (d) GS_{end} in the SMIPP for the three PFTs and all of the 27 sites. The mean values of the sensitivity coefficients are shown in asterisks.

3.3 Separating the contributions of the three indicators to annual GPP variability

As the SMIPP shows, the relative anomaly can be separated into three independent components, induced by the changes in the three indicators, respectively. Thus, the products of the relative anomalies of the three indicators by the sensitivity coefficients of annual GPP with respect to

them denote the contributions of the three indicators to annual GPP variation. Their contributions vary from site-year to site-year for each PFT (Fig. 6), which are caused by the inter-annual variation of the indicators and the variation of the sensitivity coefficients among different sites. The relative anomalies of the indicators range from -49% to 51% for GS_{start}, from -39% to 56% for GPP_{max}, and from -70% to 62% for GS_{end} among the 283 site-years. With the sensitivity coefficients for each site in Table 2, the three estimated components of annual GPP relative anomalies vary from -21% to 29% (GS_{start}), from -35% to 41% (GPP_{max}), and from -21% to 11% (GS_{end}), respectively, resulting in a range of -41% to 41% for annual GPP relative anomaly over the 283 site-years (Fig. 6). Combining the three independent components, the estimated annual GPP relative anomalies correlate well with the observed values both for a certain PFT and all sites. The NF site-years exhibit the highest R^2 (0.98), followed by ENF (0.95) and DBF (0.85) site-years, and the overall R^2 is 0.93 for the 283 site-years. The estimated annual GPP relative anomalies from GPP_{max} are much larger than those from GS_{start} and GS_{end}, indicating that GPP_{max} contributes more than GS_{start} and GS_{end} to annual GPP variability for the three PFTs (Fig. 6).

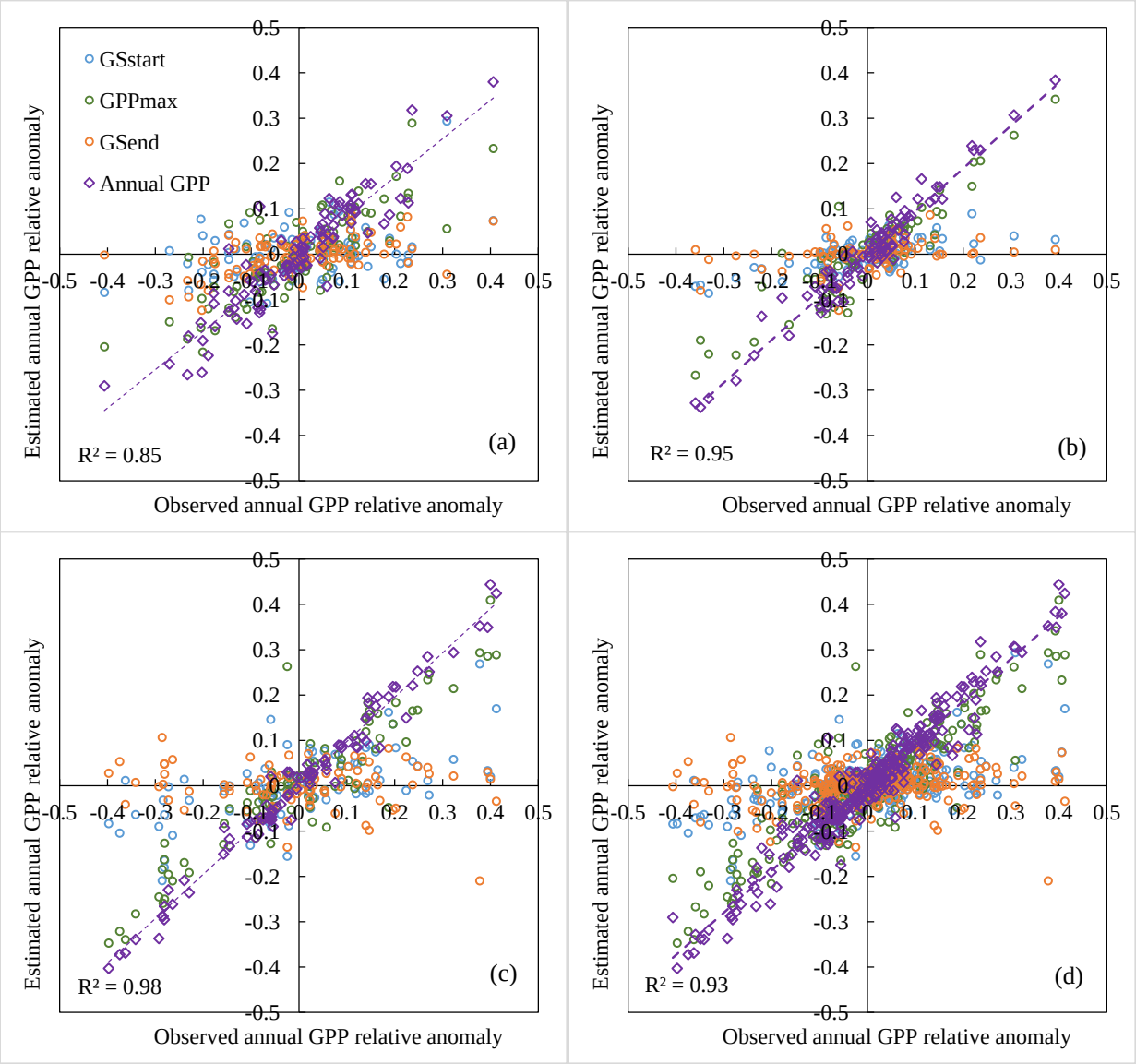

Fig. 6. Linear relationship between the observed and estimated annual GPP relative anomaly for (a) DBF; (b) ENF; (c) NF; and (d) all the 283 site-years based on the SMIPP for each site. The three components of the estimated relative anomaly induced by the three indicators are also shown.

4. Discussion

4.1 Comparison of the SMIPP with other models

In the annual cycle of vegetation growth and dormancy, GPP is controlled by photosynthetic capacity and the growing season length. Our study indicates that the three indicators are closely related to their respective seasonal GPP and the combination of them can explain annual GPP variability to a large extent. The environmental factors, such as temperature, moisture and radiation, affect annual GPP variability through their influences on the three indicators. For example, climate warming accelerates carbon assimilation in spring, which can be captured by earlier GS_{start} in view of the close relationship between warmer temperature and earlier spring emergence in temperate and boreal ecosystems (Keenan *et al.*, 2014; Piao *et al.*, 2015), and the following high temperature in summer may reduce GPP_{max} and summer GPP, because warmer temperature implies higher VPD and exacerbates soil moisture deficits during the middle of the growing season (Angert *et al.*, 2005; Buermann *et al.*, 2013). Because the three indicators can capture the fluctuations in GPP induced by changing environmental conditions, which contribute significantly to the variation in annual GPP (Zscheischler *et al.*, 2014), the proposed SMIPP is able to effectively explain annual GPP variability.

The predictive power of both phenological and physiological indicators, and the combination of them have been explored in previous studies (Richardson *et al.*, 2013; Stoy *et al.*, 2014; Wu *et al.*, 2013; Xia *et al.*, 2015). Here we compared the results of the SMIPP with three single indicator models, i.e., a simplified SMIPP version including only one indicator in equation (3) and the statistical model in Xia *et al.* (2015). The SMIPP is shown to be much more effective than any of the three single indicator models (Fig. 7). The single indicator model which only links to GPP in

the corresponding season has limitation in explaining annual GPP variability unless the seasonal GPP correlates strongly with annual GPP. For example, the three seasonal GPP is weakly correlated with annual GPP (spring: r=0.25; summer: r=0.69; autumn: r=0.40) at the US-Ne1 site, and neither of the three single indicator models can explain more than 30% of annual GPP variability. However, the combination of the three indicators in the SMIPP can effectively explain 99.5% of variation in annual GPP. Although a single indicator can capture annual GPP variation in several sites, the SMIPP can consistently explain GPP variability in most sites, indicating that annual GPP variability should be explained simultaneously from plant physiology and spring and autumn phenology.

Xia *et al.* (2015) reported that $CUP \times GPP_{max}$ well captures the variability in annual GPP, and the ratio α between annual GPP and $CUP \times GPP_{max}$ is relatively constant around 0.62 across abroad range of vegetation types and environmental conditions. In comparison with the statistical model in Xia *et al.* (2015), the SMIPP explains annual GPP variability by investigating the contributions of the three indicators to the relative change in annual GPP. Although our study does not yield any similar regression coefficients as the stable ratio α in Xia *et al.* (2015), the results indicate that the SMIPP (R^2=0.90±0.11) improves the explanatory power of Xia's model (R^2=0.87±0.16) by replacing the phenological indicator CUP with S_{start} and GS_{end} for the 27 sites (Fig. 7). This study shows that the three sensitivity coefficients vary among different sites, and the sensitivity coefficients with respect to GS_{start} and GS_{end} are not consistent for individual sites. The different sensitivity coefficients of annual GPP to GS_{start} and GS_{end} at the 27 sites indicate that the responses of annual GPP to GS_{start} and GS_{end} are not identical (Fig. 5c and d). Thus, although CUP integrates spring and autumn phenology together, it cannot fully reflect the phenological effects on annual GPP. The non-identical responses of annual GPP to

385 GS_{start} and GS_{end} may be attributed to the different environmental conditions in spring and
386 autumn, and the different triggering mechanisms of spring emergence and autumn senescence
387 (Menzel *et al.*, 2006; Vitasse *et al.*, 2009). Through distinguishing the effects of both GS_{start} and
388 GS_{end} on annual GPP, the SMIPP can better reflect the effects of plant phenological and
389 physiological changes on annual GPP change, and separate the respective contributions of
390 GS_{start}, GPP_{max}, and GS_{end} to annual GPP change based on the sensitivity coefficients of
391 annual GPP to them.

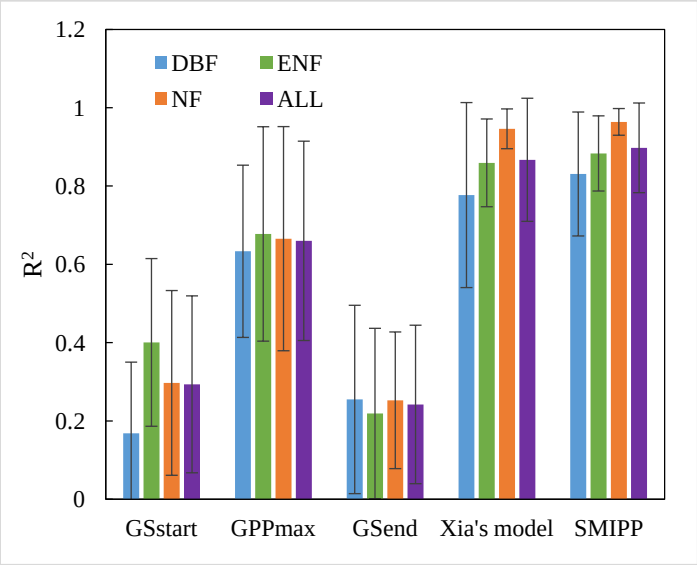

392

393 **Fig. 7.** Coefficient of determination (R^2) between the estimated and observed annual GPP
394 relative anomalies using the three single indicator models, i.e., GS_{start}, GPP_{max}, and GS_{end}, the
395 statistical model in Xia *et al.* (2015), and the SMIPP for the three PFTs and all of the 27 sites.
396 The standard deviation of the correlation coefficient is shown in black error bars.

397 **4.2 Annual GPP variability among ecosystem types**

398 The SMIPP indicates that annual GPP variability is attributed to the phenological and
399 physiological changes induced by environmental factors. The different responses of the three

indicators to environmental changes and the combined explanatory power of the three indicators to annual GPP variability are associated with ecosystem types. Correlation analyses indicate that GPP_{max} explains summer GPP the best for ENF sites, with both the highest correlation coefficient and regression slope among the three PFTs. However, GS_{start} and GS_{end} explain spring and autumn GPP the least for ENF sites. At ENF sites, where the seasonality of vegetation canopy is low, seasonal GPP variations are mainly caused by physiological changes. Both physiological and canopy (leaf-on and leaf off) changes contribute substantially to GPP variations at DBF and NF sites (Flanagan *et al.*, 2002; Gamon *et al.*, 1995; Ito *et al.*, 2006; Royer *et al.*, 2005; Saigusa *et al.*, 2002). Smaller sensitivity coefficients with respect to GS_{start} and GS_{end} are also found for ENF sites than the other two PFTs in the SMIPP. The results reported by Richardson *et al.* (2010) also indicate that the productivity of ENF is less sensitive to phenological changes than that of DBF.

In comparison with forest ecosystems, the three indicators explain annual GPP variation better for non-forest ecosystems. The partial correlation analyses present stronger relationship between each of the three indicators and annual GPP for NF than for DBF and ENF sites. In general, the distinct seasonal changes make it easier to track the changes in plant phenology and physiology, and hence annual GPP change at the NF sites. In comparison with forest ecosystems, which are more adaptive to environmental changes and can resist the environmental stresses below a certain threshold, non-forest ecosystems generally have poor self-regulation abilities under environmental stresses (Kozlowski & Pallardy, 2002; Niinemets, 2010; Teuling *et al.*, 2010). Thus, non-forests respond more quickly and intensively to environmental changes, while forests always respond to environmental changes with a delay (Zhang *et al.*, 2016). Consequently, the impact of environmental changes on annual GPP can be better captured by the three indicators,

and the SMIPP involving the three indicators can explain the inter-annual GPP variability more effectively for NF sites. The delayed and complicated responses of forests to environmental changes make it hard to track GPP variations with the three indicators at several sites, especially during drought periods.

4.3 Explanatory power of the SMIPP during drought years

Terrestrial ecosystems are closely coupled with the climate system. The carbon cycle is susceptible to climate change, and it also affects global climate through ecosystem feedback loops (Heimann & Reichstein, 2008; Luo, 2007). More and more extreme climate events have happened in recent years and significant influenced the carbon cycle (Reichstein *et al.*, 2013). Drought is one of the climate extremes which greatly reduces terrestrial carbon uptake (Allen *et al.*, 2009; Zeng *et al.*, 2005; Zhao & Running, 2010), and it brings a big challenge for the SMIPP to capture the responses to drought among different ecosystems.

Taking the 2003 European drought as an example, the four sites, i.e., IT-Ren (ENF), IT-MBo (NF), IT-Ro2 (DBF), and DE-Hai (DBF), experienced extreme drought from June through October (Ciais *et al.*, 2005). At the IT-Ren site, the forests tolerated water deficits and maintained their canopy structure during the initial phase of drought stress, and spring and summer GPP only decreased by 1.1% and 4.6%, respectively. GPP_{max}, which decreased by 5.9%, tracked the GPP decline in summer. The combination of the three indicators well explained (R^2=0.93) the annual GPP reduction of 9.7%. Warmer spring triggered more leaves and enhanced carbon uptake for NF and DBF under slight drought stress at the IT-MBo, IT-Ro2 and DE-Hai sites. Soon after they suffered severe water stress, which led to GPP decline in summer, by 14.3%, 23.4% and 11.6%, respectively. GPP_{max} emerged at early June at the three sites, more

than 10 days earlier than their mean dates, and it declined only by 4.4% at the IT-MBo and even grew by 9.9% and 4.0% at the IT-Ro2 and DE-Hai sites. Obviously, GPP_{max} did not fully reveal the drought effect on plant physiology, which reduced the explanatory power of the SMIPP.

It is worth noting that the IT-Ro2 is located in Mediterranean-climate region where drought occurs frequently in summer. During drought years, GPP dropped down in late summer and then recovered slightly in early autumn, and GPP_{max} appeared much earlier than normal years. In most sites, GPP_{max} could successfully perceive the physiological changes and reflect summer GPP variations, and the time lag between GPP_{max} and drought induced GPP decline can reduce the explanatory power of the SMIPP. It is also reported that the joint control of CUP and GPP_{max} on annual GPP variability is weak in tropical and Mediterranean climates (Xia *et al.*, 2015). On the one hand, the relationship between GPP_{max} and summer GPP is weak due to frequent summer drought; on the other hand, it is hard to determine GS_{start} and GS_{end} which can effectively reflect phenological changes in tropical and Mediterranean climates. Thus, more specified investigation into plant responses to drought is needed in order to successfully perceive the phenological and physiological changes in plants and better explain annual GPP variability in tropical and Mediterranean climates.

4.4 Limitations and implications of SMIPP under changing climate

The SMIPP works well for the ecosystems with distinct seasonal patterns, however, its explanatory power is limited in Mediterranean and tropical ecosystems. In addition, the assumption of the three independent indicators is needed in the SMIPP in order to separate the contributions of them to annual GPP variability. Although the correlation analysis in this study shows that the three indicators are independent from each other for most sites, several earlier

studies indicate that they might be interrelated as the terrestrial ecosystems respond to climate change through both phenological and physiological changes. Buermann *et al.* (2013) suggested that warming induced earlier springs may decrease summer GPP_{max} in North American boreal forests. And it was found that the timing of autumn senescence is also influenced by spring phenology in temperate deciduous forests across eastern US (Keenan & Richardson, 2015). Those phenomena are yet to be quantitatively evaluated to assess the degree of the interrelationships between the three indicators.

This study was based on the Fluxnet data at the ecosystem scale, and the SMIPP can be extended to explain and predict annual GPP variability at a regional or global scale with remote sensing data. The phenological and physiological changes can be inferred from remote sensing or webcam products to estimate annual GPP dynamics. In many studies, the phenological transitions are determined using satellite-derived vegetation indices, such as normalized difference vegetation index (NDVI) and enhanced vegetation index (EVI) (Cao *et al.*, 2015; Garrity *et al.*, 2011; Gonsamo *et al.*, 2012). The remotely derived sun-induced chlorophyll fluorescence (SIF) data are closely related to vegetation photosynthetic physiology (Damm *et al.*, 2010; Joiner *et al.*, 2014; Rossini *et al.*, 2015), and the relationship between SIF data and maximum daily GPP can be further established. Thus, the three indicators derived from remote sensing products may be used to interpret the inter-annual variability of GPP at the global scale.

5. Conclusions

This study shows that annual GPP anomaly is strongly correlated with the anomaly of GS_{start}, GPP_{max}, and GS_{end} using data from 27 flux tower sites across North America and Europe. Combining the three indicators, the SMIPP can explain 90±11% of the annual GPP variability

among the 27 sites, and it is more effective than both the single indicator models and the statistical model in Xia *et al.* (2015). For each site-year, the contributions of GS_{start}, GPP_{max}, and GS_{end} to annual GPP variation can be separated using the relative anomalies of the three indicators and the sensitivity coefficients in the SMIPP. In general, GPP_{max} contributes more than GS_{start} and GS_{end} to annual GPP variation at the 27 sites. This study indicates that the influence of climatic and environmental changes on annual GPP can be evaluated based on the three indicators within the SMIPP framework, and also elucidate that annual GPP variation can be estimated by investigating the phenological and physiological changes in terrestrial ecosystems under future climate change.

Acknowledgements

The tower flux data used for this study was obtained from the AmeriFlux (http://public.ornl.gov/ameriflux/) and EuroFlux (http://gaia.agraria.unitus.it/) networks. We acknowledge the 14 AmeriFlux and 13 EuroFlux sites (see Table 1) for their data records. In addition, funding for AmeriFlux data resources was provided by the U.S. Department of Energy's Office of Science. This study was financially supported by the National Natural Science Foundation of China (No.91125018), National Key Science and Technology Project Fund from the Ministry of Science and Technology (MOST) during the Twelfth Five-year Project (No.2013BAB05B03), and the Research and Development Special Fund for Public Welfare Industry of the Ministry of Water Research in China (No.201301081). Y. Zhang and X. Xiao are partly supported by the National Science Foundation EPSCoR research grant (IIA-1301789). The first author gratefully acknowledges the China Scholarship Council for the financial support of a 12-month study at Princeton University.

511 # References

512 Allard V, Ourcival JM, Rambal S, Joffre R, Rocheteau A (2008) Seasonal and annual variation
513 of carbon exchange in an evergreen Mediterranean forest in southern France. *Global Change*
514 *Biol.*, **14**, 714–725.

515 Allen CD, Macalady AK, Chenchouni H et al. (2009) A global overview of drought and heat
516 induced tree mortality reveals emerging climate change risk for forests. *Forest Ecol. Manag.*,
517 **259**, 660–684.

518 Angert A, Biraud S, Bonfils C et al. (2005) Drier summers cancel out the CO_2 uptake
519 enhancement induced by warmer springs. *Proc. Nat. Acad. Sci. U.S.A.*, **102**, 10823–10827.

520 Aurela M, Laurila T, Tuovinen JP (2004) The timing of snow melt controls the annual CO_2
521 balance in a subarctic fen. *Geophys. Res. Lett.*, **31**, 3–6.

522 Austin PC and Steyerberg EW (2015). The number of subjects per variable required in linear
523 regression analyses. *J. Clin. Epidemiol.*, **68**(6): 627-36.

524 Ballantyne AP, Alden CB, Miller JB, Tans PP, White JWC (2012) Increase in observed net
525 carbon dioxide uptake by land and oceans during the past 50 years. *Nature*, **488**, 70–72.

526 Bergeron O, Margolis HA, Black TA, Coursolle C, Dunn AL, Barr AG, Wofsy SC (2007)
527 Comparison of carbon dioxide fluxes over three boreal black spruce forests in Canada.
528 *Global Change Biol.*, **13**, 89–107.

529 Buermann W, Bikash PR, Jung M, Burn DH, Reichstein M (2013) Earlier springs decrease peak
530 summer productivity in North American boreal forests. *Environ. Res. Lett.*, **8**, 024027.

531 Cao R, Chen J, Shen M, Tang Y (2015) An improved logistic method for detecting spring
532 vegetation phenology in grasslands from MODIS EVI time-series data. *Agric. For. Meteorol.*,
533 **200**, 9–20.

534 Carrara A, Janssens IA, Curiel Yuste J, Ceulemans R (2004) Seasonal changes in photosynthesis,
535 respiration and NEE of a mixed temperate forest. *Agric. For. Meteorol.*, **126**, 15–31.

536 Chen H, Zhu Q, Wu N, Wang Y, Peng CH (2011) Delayed spring phenology on the Tibetan
537 Plateau may also be attributable to other factors than winter and spring warming. *Proc. Nat.*
538 *Acad. Sci. U.S.A.*, **108**, E93.

539 Churkina G, Schimel D, Braswell BH, Xiao XM (2005) Spatial analysis of growing season
540 length control over net ecosystem exchange. *Global Change Biol.*, **11**, 1777–1787.

541 Ciais P, Reichstein M, Viovy N et al. (2005) Europe-wide reduction in primary productivity
542 caused by the heat and drought in 2003. *Nature*, **437**, 529–533.

543 Cleland EE, Chuine I, Menzel A, Mooney HA, Schwartz MD (2007) Shifting plant phenology in
544 response to global change. *Trends Ecol. Evol.*, **22**, 357–365.

545 Damm A, Elber J, Erler A et al. (2010) Remote sensing of sun-induced fluorescence to improve
546 modeling of diurnal courses of gross primary production (GPP). *Global Change Biol.*, **16**,
547 171–186.

548 Dragoni D, Schmid HP, Grimmond CSB, Loescher HW (2007) Uncertainty of annual net
549 ecosystem productivity estimated using eddy covariance flux measurements. *J. Geophys.*
550 *Res.*, **112**, 1–9.

551 Dragoni D, Schmid HP, Wayson CA, Potter H, Grimmond CSB, Randolph JC (2011) Evidence
552 of increased net ecosystem productivity associated with a longer vegetated season in a
553 deciduous forest in south-central Indiana, USA. *Global Change Biol.*, **17**, 886–897.

554 Flanagan LB, Wever LA, Carlson PJ (2002) Seasonal and interannual variation in carbon dioxide
555 exchange and carbon balance in a northern temperate grassland. *Global Change Biol.*, **8**, 599–
556 615.

557 Fracheboud Y, Luquez V, Björkén L, Sjödin A, Tuominen H, Jansson S (2009) The control of
558 autumn senescence in European aspen. *Plant physiol.*, **149**, 1982–1991.

559 Fu YH, Zhao H, Piao S et al. (2015) Declining global warming effects on the phenology of
560 spring leaf unfolding. *Nature*, **526**, 104–107.

561 Gamon JA, Gamon JA, Field CB et al. (1995) Relationships between NDVI, canopy structure,
562 and photosynthesis in three California vegetation types. *Ecol. Appl.*, **5**, 28–41.

563 Garonna I, De Jong R, De Wit AJW, Mücher CA, Schmid B, Schaepman ME (2014) Strong
564 contribution of autumn phenology to changes in satellite-derived growing season length
565 estimates across Europe (1982-2011). *Global Change Biol.*, **20**, 3457–3470.

566 Garrity SR, Bohrer G, Maurer KD, Mueller KL, Vogel CS, Curtis PS (2011) A comparison of
567 multiple phenology data sources for estimating seasonal transitions in deciduous forest carbon
568 exchange. *Agric. For. Meteorol.*, **151**, 1741–1752.

569 Giasson MA, Coursolle C, Margolis HA (2006) Ecosystem-level CO_2 fluxes from a boreal
570 cutover in eastern Canada before and after scarification. *Agric. For. Meteorol.*, **140**, 23–40.

571 Gilmanov TG, Soussana JF, Aires L et al. (2007) Partitioning European grassland net ecosystem
572 CO_2 exchange into gross primary productivity and ecosystem respiration using light
573 response function analysis. *Agr. Ecosyst. Environ.*, **121**, 93–120.

574 Gioli B, Miglietta F, De Martino B et al. (2004) Comparison between tower and aircraft-based
575 eddy covariance fluxes in five European regions. *Agric. For. Meteorol.*, **127**, 1–16.

576 Gonsamo A, Chen JM, David TP, Kurz WA, Wu C (2012) Land surface phenology from optical
577 satellite measurement and CO_2 eddy covariance technique. *J. Geophys. Res. G: Biogeosci.*,
578 **117**, 1–18.

579 van Gorsel E, Delpierre N, Leuning R et al. (2009) Estimating nocturnal ecosystem respiration
580 from the vertical turbulent flux and change in storage of CO_2. *Agric. For. Meteorol.*, **149**,
581 1919–1930.

582 Groenendijk M, van der Molen MK, Dolman AJ (2009) Seasonal variation in ecosystem
583 parameters derived from FLUXNET data. *Biogeosciences Discussions*, **6**, 2863–2912.

584 Heimann M, Reichstein M (2008) Terrestrial ecosystem carbon dynamics and climate feedbacks.
585 *Nature*, **451**, 289–292.

586 Hirata R, Hirano T, Saigusa N et al. (2007) Seasonal and interannual variations in carbon dioxide
587 exchange of a temperate larch forest. *Agric. For. Meteorol.*, **147**, 110–124.

588 Hollinger DY, Aber J, Dail B et al. (2004) Spatial and temporal variability in forest-atmosphere
589 CO2 exchange. *Global Change Biol.*, **10**, 1689–1706.

590 Ibáñez I, Primack RB, Miller-Rushing AJ et al. (2010) Forecasting phenology under global
591 warming. *Philos. T. Roy. Soc. B.*, **365**, 3247–3260.

592 Ito A, Muraoka H, Koizumi H, Saigusa N, Murayama S, Yamamoto S (2006) Seasonal variation
593 in leaf properties and ecosystem carbon budget in a cool-temperate deciduous broad-leaved
594 forest: Simulation analysis at Takayama site, Japan. *Ecol. Res.*, **21**, 137–149.

595 Jeong SJ, Ho CH, Gim HJ, Brown ME (2011) Phenology shifts at start vs. end of growing season
596 in temperate vegetation over the Northern Hemisphere for the period 1982-2008. *Global*
597 *Change Biol.*, **17**, 2385–2399.

598 Joiner J, Yoshida Y, Vasilkov A et al. (2014) The seasonal cycle of satellite chlorophyll
599 fluorescence observations and its relationship to vegetation phenology and ecosystem
600 atmosphere carbon exchange. *Remote Sens. Environ.*, **152**, 375–391.

601 Keenan TF, Richardson AD (2015) The timing of autumn senescence is affected by the time of
602 spring phenology: implications for predictive models. *Global Change Biol.*, **21**, 2634-2641.

603 Keenan TF, Gray J, Friedl MA et al. (2014) Net carbon uptake has increased through warming-
604 induced changes in temperate forest phenology. *Nat. Clim. Change*, **4**, 598–604.

605 Kozlowski TT, Pallardy SG (2002) Acclimation and Adaptive Responses of Woody Plants to
606 Environmental Stresses. *Bot. Rev.*, **68**, 270–334.

Kutsch WL, Kolle O, Rebmann C, Knohl A, Ziegler W, Schulze ED (2008) Advection and resulting CO_2 exchange uncertainty in a tall forest in central Germany. *Ecol. Appl.*, **18**, 1391–1405.

Liang S, Zheng T, Liu R, Fang H, Tsay SC, Running S (2006) Estimation of incident photosynthetically active radiation from Moderate Resolution Imaging Spectrometer data. *J. Geophys. Res.*, **111**, 1–13.

Lund M, Lafleur PM, Roulet NT et al. (2010) Variability in exchange of CO_2 across 12 northern peatland and tundra sites. *Global Change Biol.*, **16**, 2436–2448.

Luo Y (2007) Terrestrial Carbon–Cycle Feedback to Climate Warming. *Annu. Rev. Ecol. Evol. S.*, **38**, 683–712.

Luo Y, Keenan TF, Smith M (2015) Predictability of the terrestrial carbon cycle. *Global Change Biol.*, **21**, 1737-1751.

Menzel A, Fabian P (1999) Growing season extended in Europe. *Nature*, **397**, 659.

Menzel A, Sparks TH, Estrella N et al. (2006) European phenological response to climate change matches the warming pattern. *Global Change Biol.*, **12**, 1969–1976.

Nave LE, Gough CM, Maurer KD et al. (2011) Disturbance and the resilience of coupled carbon and nitrogen cycling in a north temperate forest. *J. Geophys. Res. G: Biogeosci.*, **116**, 1–14.

Niinemets Ü (2010) Responses of forest trees to single and multiple environmental stresses from seedlings to mature plants: Past stress history, stress interactions, tolerance and acclimation. *Forest Ecol. Manag.*, **260**, 1623–1639.

Panchen ZA, Primack RB, Gallinat AS, Nordt B, Stevens A, Du Y, Fahey R (2015) Substantial variation in leaf senescence times among 1360 temperate woody plant species: implications for phenology and ecosystem processes. *Ann. Bot.*, **116**, 865-873.

Papale D, Valentini R (2003) A new assessment of European forests carbon exchanges by eddy fluxes and artificial neural network spatialization. *Global Change Biol.*, **9**, 525–535.

Piao S, Friedlingstein P, Ciais P, Viovy N, Demarty J (2007) Growing season extension and its impact on terrestrial carbon cycle in the Northern Hemisphere over the past 2 decades. *Global Biogeochem. Cycles*, **21**, GB3018.

Piao, S. et al., 2015. Leaf onset in the northern hemisphere triggered by daytime temperature. *Nat. Commun.*, **6**, 6911.

Pope KS, Dose V, Da Silva D, Brown PH, Leslie CA, Dejong TM (2013) Detecting nonlinear response of spring phenology to climate change by Bayesian analysis. *Global Change Biol.*, **19**, 1518–1525.

Reichstein M, Falge E, Baldocchi D et al. (2005) On the separation of net ecosystem exchange into assimilation and ecosystem respiration: Review and improved algorithm. *Global Change Biol.*, **11**, 1424–1439.

Reichstein M, Bahn M, Ciais P et al. (2013) Climate extremes and the carbon cycle. *Nature*, **500**, 287–95.

Richardson AD, Black TA, Ciais P et al. (2010) Influence of spring and autumn phenological transitions on forest ecosystem productivity. *Philos. T. Roy. Soc. B.*, **365**, 3227–46.

Richardson AD, Hollinger DY (2005) Statistical modeling of ecosystem respiration using eddy covariance data: Maximum likelihood parameter estimation, and Monte Carlo simulation of model and parameter uncertainty, applied to three simple models. *Agric. For. Meteorol.*, **131**, 191–208.

Richardson AD, Keenan TF, Migliavacca M, Ryu Y, Sonnentag O, Toomey M (2013) Climate change, phenology, and phenological control of vegetation feedbacks to the climate system. *Agric. For. Meteorol.*, **169**, 156–173.

Rossini M, Nedbal L, Guanter L et al. (2015) Red and far red Sun-induced chlorophyll fluorescence as a measure of plant photosynthesis. *Geophys. Res. Lett.*, **42**, 1632–1639.

Royer DL, Osborne CP, Beerling DJ (2005) Contrasting seasonal patterns of carbon gain in evergreen and deciduous trees of ancient polar forests. *Paleobiology*, **31**, 141–150.

Saigusa N, Yamamoto S, Murayama S, Kondo H, Nishimura N (2002) Gross primary production and net ecosystem exchange of a cool-temperate deciduous forest estimated by the eddy covariance method. *Agric. For. Meteorol.*, **112**, 203–215.

Saigusa N, Yamamoto S, Hirata R et al. (2008) Temporal and spatial variations in the seasonal patterns of CO_2 flux in boreal, temperate, and tropical forests in East Asia. *Agric. For. Meteorol.*, **148**, 700–713.

Saito M, Maksyutov S, Hirata R, Richardson AD (2009) An empirical model simulating long-term diurnal CO_2 flux for diverse vegetation types. *Biogeosciences*, **6**, 585–599.

Schwalm CR, Williams CA, Schaefer K et al. (2012) Reduction in carbon uptake during turn of the century drought in western North America. *Nat. Geosci.*, **5**, 551–556.

Scurlock JMO, Johnson K, Olson RJ (2002) Estimating net primary productivity from grassland biomass dynamics measurements. *Global Change Biol.*, **8**, 736–753.

Stoy PC, Mauder M, Foken T et al. (2013) A data-driven analysis of energy balance closure across FLUXNET research sites: The role of landscape scale heterogeneity. *Agric. For. Meteorol.*, **171-172**, 137–152.

673 Stoy PC, Trowbridge AM, Bauerle WL (2014) Controls on seasonal patterns of maximum
674 ecosystem carbon uptake and canopy-scale photosynthetic light response: Contributions from
675 both temperature and photoperiod. *Photosynth. Res.*, **119**, 49–64.

676 Suyker AE, Verma SB, Burba GG, Arkebauer TJ (2005) Gross primary production and
677 ecosystem respiration of irrigated maize and irrigated soybean during a growing season.
678 *Agric. For. Meteorol.*, **131**, 180–190.

679 Teuling AJ, Seneviratne SI, Stöckli R et al. (2010) Contrasting response of European forest and
680 grassland energy exchange to heatwaves. *Nat. Geosci.*, **3**, 722–727.

681 Thum T, Aalto T, Laurila T, Aurela M, Kolari P, Hari P (2007) Parametrization of two
682 photosynthesis models at the canopy scale in a northern boreal Scots pine forest. *Tellus B.*,
683 **59**, 874–890.

684 Uehlinger U (2006) Annual cycle and inter-annual variability of gross primary production and
685 ecosystem respiration in a floodprone river during a 15-year period. *Freshwater Biol.*, **51**,
686 938–950.

687 Urbanski S, Barford C, Wofsy S et al. (2007) Factors controlling CO_2 exchange on timescales
688 from hourly to decadal at Harvard Forest. *J. Geophys. Res. G: Biogeosci.*, **112**, 1–25.

689 Valentini R, DeAngelis P, Matteucci G, Monaco R, Dore S, Mugnozza GES (1996) Seasonal net
690 carbon dioxide exchange of a beech forest with the atmosphere. *Global Change Biol.*, **2**,
691 199–207.

692 Vautard R, Yiou P, Ghil M (1992) Singular-spectrum analysis: A toolkit for short, noisy chaotic
693 signals. *Physica. D.*, **58**, 95–126.

694 Vitasse Y, Porté AJ, Kremer A, Michalet R, Delzon S (2009) Responses of canopy duration to
695 temperature changes in four temperate tree species: Relative contributions of spring and
696 autumn leaf phenology. *Oecologia*, **161**, 187–198.

697 Wohlfahrt G, Anderson-Dunn M, Bahn M et al. (2008) Biotic, abiotic, and management controls
698 on the net ecosystem CO_2 exchange of European mountain grassland ecosystems.
699 *Ecosystems*, **11**, 1338–1351.

700 Wu C, Chen JM, Black TA et al. (2013) Interannual variability of net ecosystem productivity in
701 forests is explained by carbon flux phenology in autumn. *Global Ecol. and Biogeogr.*, **22**,
702 994–1006.

703 Xia J, Niu S, Ciais P et al. (2015) Joint control of terrestrial gross primary productivity by plant
704 phenology and physiology. *Proc. Nat. Acad. Sci. U.S.A.*, **112**, 2788–2793.

705 Yang Y, Guan H, Shen M, Liang W, Jiang L (2015) Changes in autumn vegetation dormancy

706 onset date and the climate controls across temperate ecosystems in China from 1982 to 2010.
707 *Global Change Biol.*, **21**, 652–665.

708 Yi C, Davis KJ, Bakwin PS et al. (2004) Observed covariance between ecosystem carbon
709 exchange and atmospheric boundary layer dynamics at a site in northern Wisconsin. *J.*
710 *Geophys. Res. D: Atmos.*, **109**, 1–9.

711 Yi S, Zhou Z (2011) Increasing contamination might have delayed spring phenology on the
712 Tibetan Plateau. *Proc. Nat. Acad. Sci. U.S.A.*, **108**, E94; author reply E95.

713 Yu H, Luedeling E, Xu J (2010) Winter and spring warming result in delayed spring phenology
714 on the Tibetan Plateau. *Proc. Nat. Acad. Sci. U.S.A.*, **107**, 22151–22156.

715 Zeng N, Qian H, Roedenbeck C, Heimann M (2005) Impact of 1998-2002 midlatitude drought
716 and warming on terrestrial ecosystem and the global carbon cycle. *Geophys. Res. Lett.*, **32**, 1–
717 4.

718 Zhang Y, Xiao X, Zhou S, Ciais P, McCarthy H, Luo Y (2016) Canopy and physiological
719 limitation of GPP during drought and heat wave. *Geophys. Res. Lett.*, **43**, 3325–3333.

720 Zhao M, Running SW (2010) Drought-Induced Reduction in Global terrestrial net primary
721 production from 2000 through 2009. *Science*, **329**, 940–943.

722 Zhu W, Tian H, Xu X, Pan Y, Chen G, Lin W (2012) Extension of the growing season due to
723 delayed autumn over mid and high latitudes in North America during 1982-2006. *Global Ecol.*
724 *Biogeogr.*, **21**, 260–271.

725 Zscheischler J et al. (2014) A few extreme events dominate global interannual variability in
726 gross primary production. *Environ. Res. Lett.*, **9**, 035001.

727 Zweifel R, Eugster W, Etzold S, Dobbertin M, Buchmann N, Häsler R (2010) Link between
728 continuous stem radius changes and net ecosystem productivity of a subalpine Norway
729 spruce forest in the Swiss Alps. *New Phytol.*, **187**, 819–830.